The Relationship between the Crystal Structure and Electrical Properties of Oxide Ion Conducting $Ba_3W_{1.2}Nb_{0.8}O_{8.6}$

Kirstie S. McCombie [1], Eve J. Wildman [1], Clemens Ritter [2], Ronald I. Smith [3], Janet M. S. Skakle [1] and Abbie C. Mclaughlin [1]*

[1] Department of Chemistry, University of Aberdeen, Meston Walk, Aberdeen AB24 3UE, United Kingdom

[2] Institut Laue Langevin, 71 Avenue de Martyrs, BP 156, F-38042 Grenoble Cedex 9, France

[3] ISIS Facility, Rutherford Appleton Laboratory, Harwell, Didcot OX11 0DE, UK

ABSTRACT

The oxide ionic conductor $Ba_3W_{1.2}Nb_{0.8}O_{8.6}$ has been synthesised as part of an investigation into the new class of $Ba_3M'M''O_{8.5}$ (M' = W, Mo; M'' = Nb) oxide-ion conducting hexagonal perovskite derivatives. The substitution of W^{6+} for Nb^{5+} in $Ba_3W_{1+x}Nb_{1-x}O_{8.5+x/2}$ leads to an increase in the oxygen content, which enhances the low temperature ionic conductivity. However at 400 °C, the ionic conductivity of $Ba_3W_{1.2}Nb_{0.8}O_{8.6}$ is still significantly lower than the molybdenum compound $Ba_3MoNbO_{8.5}$. Remarkably, at 600 °C the bulk oxide ionic conductivities of $Ba_3MoNbO_{8.5}$, $Ba_3WNbO_{8.5}$ and $Ba_3W_{1.2}Nb_{0.8}O_{8.6}$ are very similar (σ_b = 0.0016 S cm^{-1}, 0.0017 S cm^{-1} and 0.0022 S cm^{-1} respectively). The variable temperature neutron diffraction results reported here demonstrate that $Ba_3W_{1.2}Nb_{0.8}O_{8.6}$ undergoes a similar structural rearrangement to $Ba_3MoNbO_{8.5}$ above 300 °C but the ratio of $(W/Nb)O_4$ tetrahedra to $(W/Nb)O_6$ octahedra rises at a faster rate upon heating between 300 and 600 °C. There is a clear relationship between the ionic conductivity of $Ba_3M'_{1+x}M''_{1-x}O_{8.5+x/2}$ (M' = W, Mo; M''

= Nb) phases and the number of tetrahedrally coordinated *M′* and *M″* cations present within the crystal structure.

INTRODUCTION

Interest in oxide ion conducting materials has recently increased due to their many applications, including electrolytes in solid oxide fuel cells (SOFCs) and oxygen separation membranes. [1-4] Efficiencies greater than 85% have been achieved in SOFCs in combined heat and power applications. [5, 6] Additionally, SOFCs are fuel-flexible with negligible emissions of CO_2 and NO_x gases produced. [7] An important goal is to reduce the high temperature of operation of SOFCs to 400 – 650 °C, whilst still realizing sufficient conductivities comparable to those achieved using zirconia-based electrolytes. [8] New materials are therefore sought which can exhibit high oxide ion conductivities at lower temperatures.

Fast oxide ion conductivity has been observed in several crystal structure types, including fluorite-related structures; [4, 9] $La_2Mo_2O_9$ (LAMOX) based materials; [10] $Bi_4V_2O_{11}$ based oxides; [11] lanthanum silicate and germanate apatites; [12] perovskites [13, 14] and the perovskite derivative $NdBaInO_4$. [15] There are also several accounts of hexagonal perovskites which exhibit mixed electronic and ionic conductivity, including $Ba_7Y_2Mn_3Ti_2O_{20}$ [16] and the compounds $Ba_4M_2O_9$ (M = Nb, Ta, Sb). [17-19] Significant oxide ion conductivity has recently been identified in $Ba_3MoNbO_{8.5}$ [20] and $Ba_3WNbO_{8.5}$ [21], which exhibit bulk conductivities of 2.2 x 10^{-3} S cm^{-1} and 1.7 x 10^{-3} S cm^{-1}, respectively, at 600 °C. These compounds crystallise in a hybrid of the 9R hexagonal perovskite and palmierite structures, [20] containing a disordered mixture of $(M/Nb)O_4$ tetrahedra and $(M/Nb)O_6$ octahedra (M = W, Mo) and hence intrinsic oxygen vacancies. The results of a neutron diffraction study have demonstrated that, above 300 °C, $Ba_3MoNbO_{8.5}$ undergoes a structural rearrangement and the ionic conductivity is enhanced as the number of $(Mo/Nb)O_4$ tetrahedra within the average structure increases. [22]

$Ba_3Mo_{1-x}Nb_{1+x}O_{8.5-x/2}$ (x = 0 – 0.2) have also been synthesized. The substitution of Nb^{5+} for Mo^{6+} results in a reduced percentage of $(Mo/Nb)O_4$ tetrahedra lowering the oxide ionic conductivity between 300 – 500 °C. [23] However, the bulk oxide ionic conductivities of the $Ba_3Mo_{1-x}Nb_{1+x}O_{8.5-x/2}$ phases are very similar at 600 °C. Similarly at 450 °C the bulk conductivity of $Ba_3WNbO_{8.5}$ is more than an order of magnitude lower than that of $Ba_3MoNbO_{8.5}$ but at 600 °C the bulk ionic conductivities of both compounds are comparable. [21] It has been suggested that the same structural rearrangement previously reported for $Ba_3MoNbO_{8.5}$ occurs in these compounds, preserving the high-temperature ionic conductivity. [21, 22]

In the work reported here, we examine further the relationship between the ratio of $(W/Nb)O_4$ tetrahedra to $(W/Nb)O_6$ octahedra, temperature and conductivity. The W/Nb ratio was altered so as to adjust the oxygen stoichiometry according to

$$Nb^{5+} \rightarrow W^{6+} + \tfrac{1}{2} O^{2-}$$

resulting in the synthesis of $Ba_3W_{1.2}Nb_{0.8}O_{8.6}$. The electrical properties of this limiting composition were measured using electrochemical impedance spectroscopy (EIS), and a variable temperature neutron diffraction study was performed in order to investigate structure-property relationships in $Ba_3W_{1.2}Nb_{0.8}O_{8.6}$. The results demonstrate that upon heating to 600 °C there is an increase in the ratio of $(W/Nb)O_4$ tetrahedra to $(W/Nb)O_6$ octahedra, enhancing the bulk conductivity.

EXPERIMENTAL

Compositions in the solid solution $Ba_3W_{1+x}Nb_{1-x}O_{8.5+x/2}$ (x = 0.05, 0.10, 0.20 and 0.33) were prepared as reported previously for $Ba_3WMnO_{8.5}$ [21]. The heating step at 1300 °C was repeated three times until the compound was phase pure.

X-ray powder diffraction patterns were collected at room temperature on a PANalytical Empyrean Powder diffractometer between 5° < 2θ < 70°, with a step size of 0.0131°.

In order to accurately determine the oxygen atom positions and fractional occupancies, time-of-flight (TOF) neutron powder diffraction data were collected at ~ 25 °C on the General Materials (GEM) Diffractometer at the ISIS pulsed neutron source, Rutherford Appleton Laboratory, UK. 5 g of $Ba_3W_{1.2}Nb_{0.8}O_{8.6}$ were loaded into an 8 mm diameter vanadium can and data were acquired in all six detector banks for a period of 350 microAmp hours, corresponding to ~ 2 hours data collection.

Variable temperature neutron diffraction data were recorded on the high resolution powder diffractometer D2B at the Institut Laue-Langevin (ILL) in Grenoble. A sample of ~ 3 g of $Ba_3W_{1.2}Nb_{0.8}O_{8.6}$ was inserted into an open quartz tube and data were collected between 100 °C and 600 °C at λ = 1.59432 Å in the range of 5° < 2θ < 160°, with a total scan time of 2.75 hours at each temperature.

Rietveld refinements were performed using the GSAS/EXPGUI programme. [24, 25] At each temperature the scale factor, background (shifted Chebyschev polynomial function), pseudo-Voigt profile function, lattice parameters, zero shift, atomic coordinates and anisotropic displacement parameters were refined. The hybrid 9R polytype – palmierite crystal structure previously reported for $Ba_3MoNbO_{8.5}$ [20] and $Ba_3WNbO_{8.5}$ [21] was used as a starting model. The O(1) and Ba fractional occupancies refined to within 1% of full occupancy and were fixed at 1.0 in further refinement. The occupancies of all other atoms were freely refined. The total occupancy of the Nb and W positions was fixed to fit the stoichiometry.

Impedance spectroscopy measurements were performed on a pellet of 10 mm diameter with 92% of the theoretical density. Data were recorded with a Solartron 1260 impedance analyser

in the frequency range 0.1 Hz – 1 MHz. The sample was cooled from 600 °C to 400 °C in steps of 15 °C and equilibrated for 2 hours at each temperature. Data were recorded under a dry flow of air, pure nitrogen, pure oxygen and 5 % hydrogen/nitrogen and processed with the ZView software.

RESULTS AND DISCUSSION

Preliminary Characterisation

Only the x = 0.2 phase could be successfully synthesised as a pure phase at 1300 °C, despite the synthesis of x = 0.33 being reported previously. [26] Repeated attempts to prepare compounds with x = 0.05, 0.10 and 0.33 resulted in samples containing impurities of both $BaWO_4$ (space group $I4_1/a$; a = 5.6065(7) Å and c = 12.7084(16) Å [27]) and $Ba_9Nb_6WO_{27}$ (space group $R\bar{3}m$ H (a = 5.790(1), c = 63.400(1) [28]). The X-ray diffraction patterns of the $Ba_3W_{1+x}Nb_{1-x}O_{8.5+x}$ phases are displayed in Figure S1. The reason for the stability of the x = 0.2 phase is currently unknown and theoretical calculations are warranted as they will give valuable insight for further doping strategies.

The X-ray diffraction pattern of $Ba_3W_{1.2}Nb_{0.8}O_{8.6}$ was indexed with the space group $R\bar{3}m$ H (a = 5.8570 (1) Å and c = 20.9964 (5) Å), as previously reported for $Ba_3WNbO_{8.5}$.[21] The $Ba_3W_{1.2}Nb_{0.8}O_{8.6}$ phase is stable at 600 °C in N_2, O_2 and 5 % H_2/N_2 (Figure S2).

Electrical Characterisation

Typical impedance spectra of $Ba_3W_{1.2}Nb_{0.8}O_{8.6}$ at 400 °C and 600 °C are displayed as Nyquist plots in Figure S3. A Warburg electrode response is observed at all temperatures above 400 °C in the low frequency region (<10 Hz). Such a response is indicative of ionic conduction in a material with partially blocking electrodes. [29]. The bulk and grain boundary responses overlap

at all temperatures as previously reported for $Ba_3WNbO_{8.5}$. [21] Equivalent circuit analysis was achieved using the same model described for $Ba_3WNbO_{8.5}$. [21] The fit to this model is shown in Figure S3. The capacitance values were calculated as $C_b \sim 3.6$ pF cm^{-1} and $C_{gb} \sim 0.014$ nF cm^{-1}.

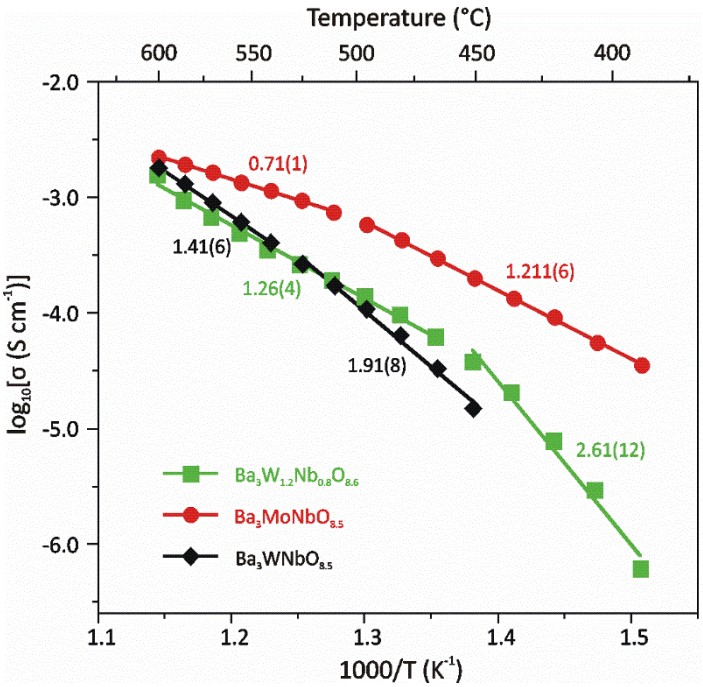

Figure 1. Arrhenius plot of the bulk (σ_b) conductivities of $Ba_3W_{1.2}Nb_{0.8}O_{8.6}$, $Ba_3MoNbO_{8.5}$ and $Ba_3WNbO_{8.5}$. Data for $Ba_3MoNbO_{8.5}$ and $Ba_3WNbO_{8.5}$ are taken from references 20 and 21 respectively. Activation energies (in eV) are shown on the figure.

The Arrhenius plot of the bulk conductivities of $Ba_3W_{1.2}Nb_{0.8}O_{8.6}$ $Ba_3WNbO_{8.5}$ [21] and $Ba_3MoNbO_{8.5}$ [20] are presented in Figure 1. The bulk conductivity of $Ba_3W_{1.2}Nb_{0.8}O_{8.6}$ is 0.0016 S cm^{-1} at 600 °C. A change in gradient is observed above 450 °C, so that the bulk activation energy decreases from 2.61 ± 0.12 eV to 1.26 ± 0.04 eV. Similar changes in slope are observed for $Ba_3MoNbO_{8.5}$ [20] and $Ba_3WNbO_{8.5}$. [21] The bulk conductivity of $Ba_3W_{1.2}Nb_{0.8}O_{8.6}$ is higher than that of $Ba_3WNbO_{8.5}$ at 400 °C but much lower than that of $Ba_3MoNbO_{8.5}$ (Fig. 1). At 600 °C the

bulk conductivities of $Ba_3W_{1.2}Nb_{0.8}O_{8.6}$, $Ba_3WNbO_{8.5}$ and $Ba_3MoNbO_{8.5}$ are very similar (σ_b = 0.0016 S cm^{-1}, 0.0017 S cm^{-1} and 0.0022 S cm^{-1} at 600°C respectively).

The Arrhenius plot of the total conductivity of $Ba_3W_{1.2}Nb_{0.8}O_{8.6}$ in several different atmospheres is displayed in Figure S4. The results demonstrate that, like $Ba_3WNbO_{8.5}$, [21] $Ba_3W_{1.2}Nb_{0.8}O_{8.6}$ exhibits negligible electronic conductivity from 400 °C – 600 °C over the pO_2 range measured. The grain boundary resistivity dominates the total resistivity of $Ba_3W_{1.2}Nb_{0.8}O_{8.6}$ (σ_{gb} = 3.7 x 10^{-5} S cm^{-1} at 600 °C. The activation energy is 1.268 ± 0.006 eV). Materials containing barium that are sintered at high temperature can have a different chemical composition of the grain boundaries resulting in a higher grain boundary resistivity. [30] This is caused by barium vaporisation and/or segregation of secondary phases such as $BaCO_3$ in the grain boundaries. Further sintering studies will be required in order to reduce the grain boundary resistivity and further exploit the high bulk conductivity of these materials.

Crystal structure of $Ba_3W_{1.2}Nb_{0.8}O_{8.6}$

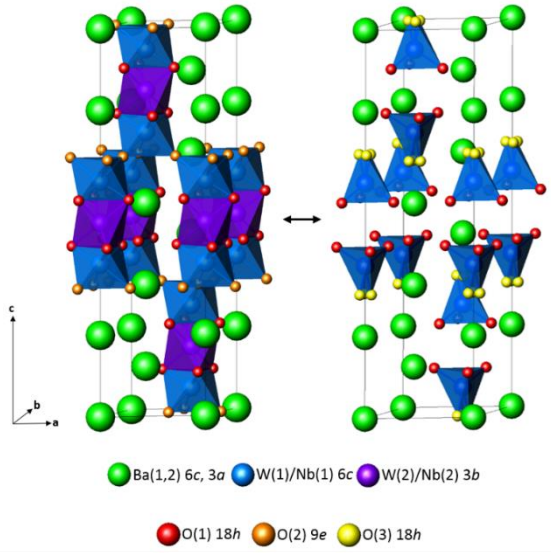

Figure 2. The hybrid crystal structure of $Ba_3W_{1.2}Nb_{0.8}O_{8.6}$.

a

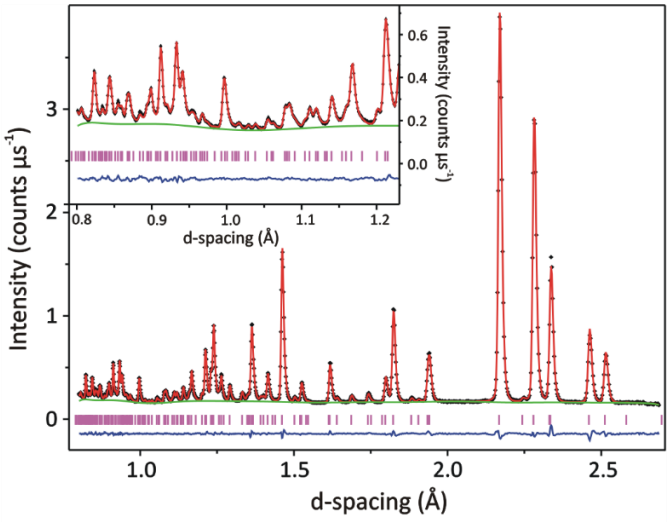

b

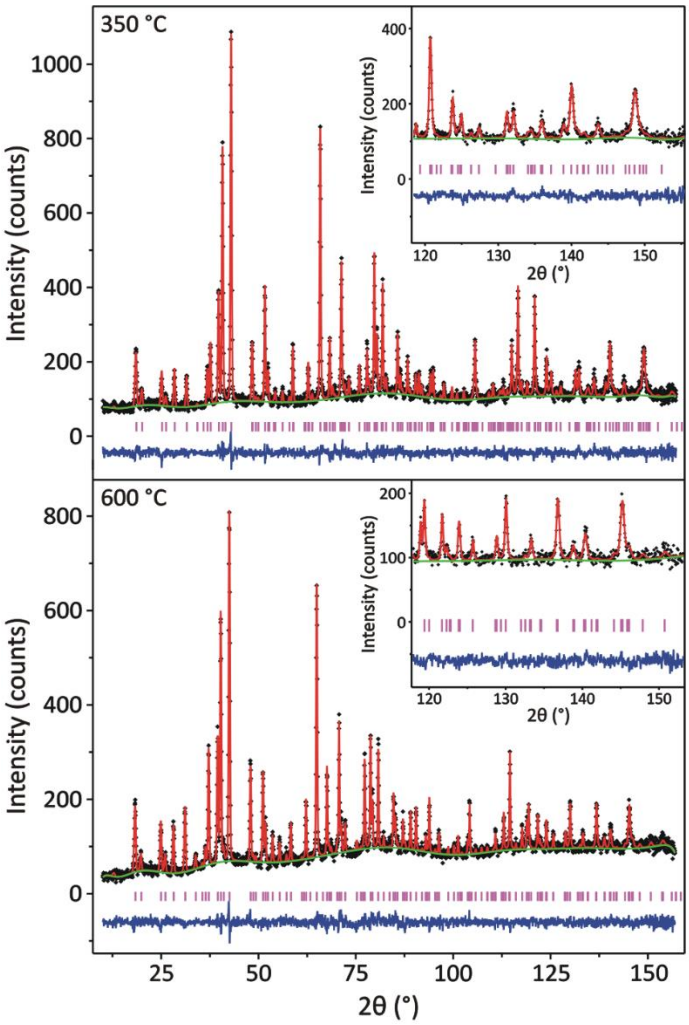

Figure 3. (a) Fitted room temperature TOF powder neutron diffraction pattern from $Ba_3W_{1.2}Nb_{0.8}O_{8.6}$ collected on the GEM 2θ ~ 90° detector bank. (b) Fitted powder neutron diffraction patterns collected at 350°C and 600 °C on the D2B diffractometer.

A good Rietveld fit to the hybrid model shown in Figure 2 was obtained at 25 °C (Figure 3(a)). Disorder of the oxygen atom, O(3) is observed as previously reported for $Ba_3WNbO_{8.5}$. [21] The agreement indices and refined atomic positions are shown in Table S1. Highly anisotropic thermal displacement of the W/Nb cations along the c-axis is observed (Table S1). Similar U_{ij} values have been reported for $Ba_3WNbO_{8.5}$ and $Ba_3MoNbO_{8.5}$. [20, 21]

At 25 °C there are ~ 13% of W(1)/Nb(1)O_4 tetrahedra within the average structure of $Ba_3W_{1.2}Nb_{0.8}O_{8.6}$ in contrast to~ 50% of Mo(1)/Nb(1)O_4 tetrahedra in $Ba_3MoNbO_{8.5}$. There are also 13% of W(1)/Nb(1)O_4 tetrahedra present in the average structure of $Ba_3WNbO_{8.5}$ [21]. There is an increase in the oxygen content upon substitution of W^{6+} for Nb^{5+} in $Ba_3W_{1+x}Nb_{1-x}O_{8.5+x/2}$ (x = 0.2). Results from Rietveld refinement demonstrate that the extra oxygen is located at the O(2) site at 25 °C. There is no change in the fractional occupancy of the O(3) site. [21] The increase in oxygen content results in a reduction in the number of mobile oxygen ion vacancies (charge carriers) in the $BaO_{2.6}$ layers (Figure 3), where the ionic conductivity is thought to originate. [20] The bulk conductivity of $Ba_3W_{1.2}Nb_{0.8}O_{8.6}$ is greater than that of $Ba_3WNbO_{8.5}$ at 400 °C ($\sigma_{\mathbf{b}}$= 3.0 x 10^{-6} S cm^{-1} and 4.8 x 10^{-7} S cm^{-1} respectively (Figure 1)), which would suggest that the number of charge carriers in $Ba_3WNbO_{8.5}$ is not optimum and could potentially be further enhanced by increasing the oxygen content via chemical doping. At the same time the substitution of W^{6+} for Nb^{5+} results in a higher fractional occupancy of the M(1) site (the fractional occupancies of the M(1) site are 0.91 and 0.82 for $Ba_3W_{1.2}Nb_{0.8}O_{8.6}$ and $Ba_3WNbO_{8.5}$ [21] respectively). It was not possible to determine the ratio of W:Nb at the M(1) and M(2) sites and X-ray absorption experiments are warranted to gain more insight into the local co-ordination environments.

It has been postulated that the reason the bulk conductivities of $Ba_3MoNbO_{8.5}$, $Ba_3WNbO_{8.5}$ and $Ba_3Mo_{1-x}Nb_{1+x}O_{8.5-x/2}$ are similar at 600 °C is a result of a different rate of change in O(2), O(3), M(1) and M(2) fractional occupancies upon heating [21, 23], so that the ratio of $(M/Nb)O_4$ tetrahedra to $(M/Nb)O_6$ octahedra is comparable in all compounds at 600°C. In order to verify this theory, variable temperature neutron diffraction data were collected on $Ba_3W_{1.2}Nb_{0.8}O_{8.6}$ between 25 °C and 600 °C.

The Rietveld refinement fits at 350 °C and 600 °C are displayed in Figure 3 (b). The $R\bar{3}m$ H space group is observed at all temperatures. The variation of the *a* and *c* cell parameters with temperature is displayed in Figure 4. Non-monotonic behaviour is clearly observed.

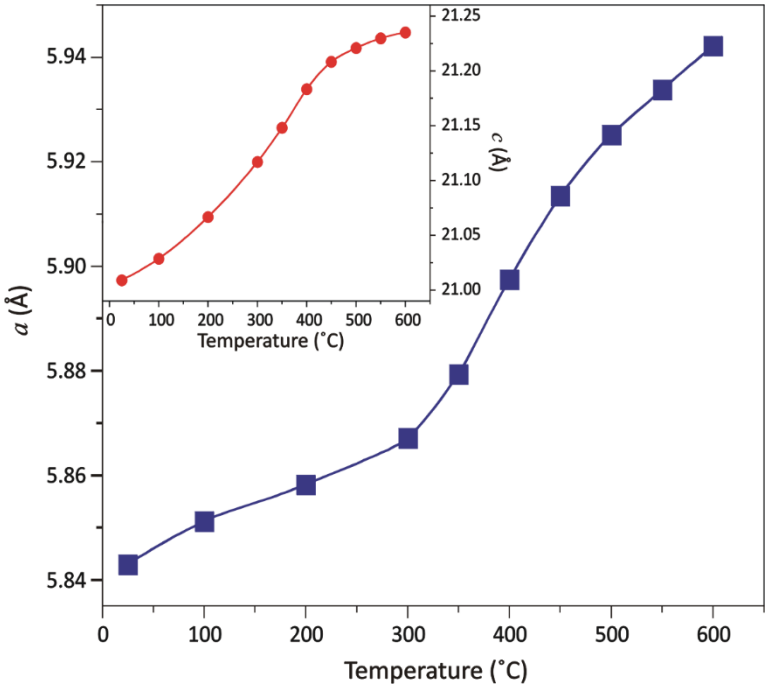

Figure 4. The thermal variation of the *a* cell parameter. The inset shows the thermal evolution of the *c* cell parameter.

The variation of the O(2), O(3), M(1) and M(2) fractional occupancies with temperature are displayed in Figure 5. Clear changes in the fractional occupancies are observed above 300 °C. The O(3) and M(1) fractional occupancies both increase above 300 °C, whilst the O(2) and

M(2) fractional occupancies decrease. The results demonstrate that above 300 °C the crystal structure rearranges, resulting in an increase in the percentage of $(W,Nb)O_4$ tetrahedra within the average structure. The same structural rearrangement has been reported for $Ba_3MoNbO_{8.5}$ [22] and results in an enhancement of the bulk ionic conductivity. [22]

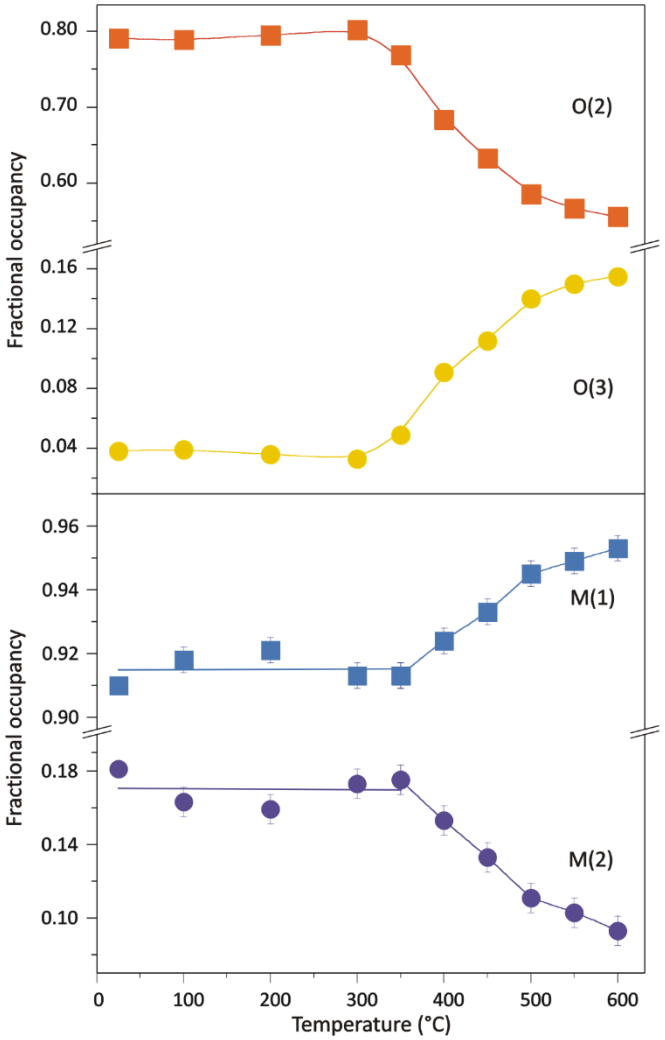

Figure 5. The thermal evolution of the M(1), M(2), O(2) and O(3) fractional occupancies.

The Arrhenius plot of the bulk conductivity combined with the variation of the fractional occupancy of O(3) with temperature of $Ba_3W_{1.2}Nb_{0.8}O_{8.6}$ are presented in Figure 6, demonstrating that there is a relationship between the thermal evolution of the crystal structure and the electrical properties. Below 300 °C, the percentage of tetrahedra in

$Ba_3W_{1.2}Nb_{0.8}O_{8.6}$ is ~ 13.0% and increases to ~ 41.8% at 500 °C and ~ 45.5% at 600 °C. In contrast there are ~ 51.3% tetrahedra within the average structure of $Ba_3MoNbO_{8.5}$ at 300 °C which increases to ~ 64.5% at 500 °C and ~ 64.9% at 600 °C [22]. This shows that the rate of increase of the $(W,Nb)O_4$ tetrahedra upon heating from 300 °C to 600 °C is faster in $Ba_3W_{1.2}Nb_{0.8}O_{8.6}$ than in $Ba_3MoNbO_{8.5}$ enhancing the bulk conductivity at 600 °C (Figure 1). Moreover in corroboration, Bernasconi *et al.* have recently reported a variable temperature synchrotron high resolution X-ray diffraction study of $Ba_3Mo_{1-x}W_xNbO_{8.5}$ (x = 0, 0.25, 0.50, 0.75 and 1.0) [31] where they report a similar relationship between the evolution of the crystal structure and the bulk ionic conductivity.

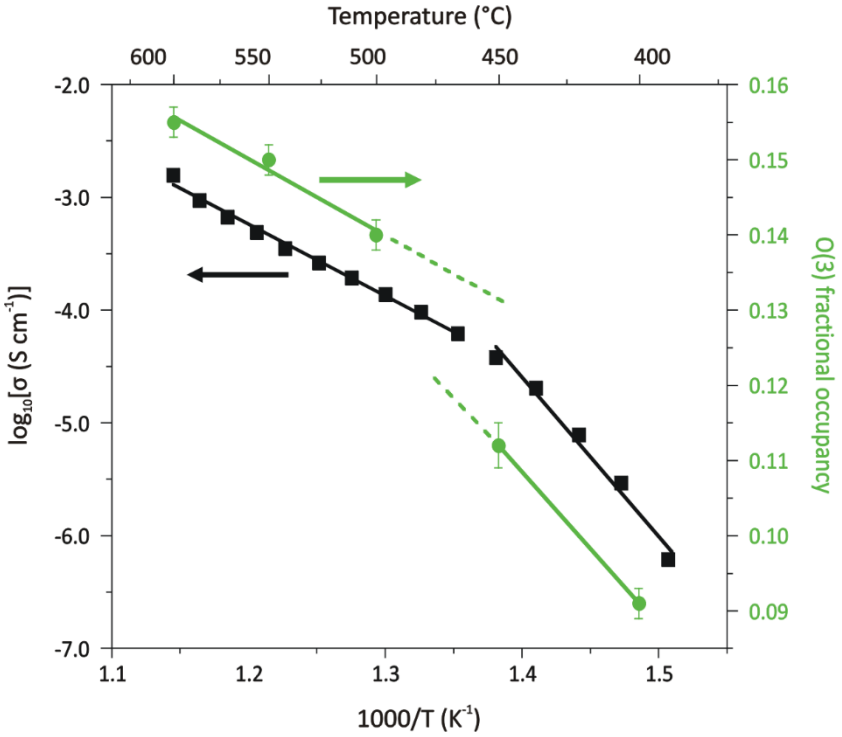

Figure 6. The thermal variation of the O(3) fractional occupancy combined with the Arrhenius plot of the bulk conductivity of $Ba_3W_{1.2}Nb_{0.8}O_{8.6}$.

The bond lengths and angles calculated from the Rietveld refinements are displayed in Supplementary Tables S2-S3. The structural rearrangement above 300 °C is clearly evidenced in the changes in cell parameters and bond lengths and angles within the $M(1)O_x$ polyhedra as the structure relaxes (Figure S5). The thermal evolution of the bond lengths and angles are comparable to those previously described for $Ba_3MoNbO_{8.5}$. [22] The $Ba_3M'_{1+x}M''_{1-x}O_{8.5+x/2}$ (*M'* = W, Mo; *M''* = Nb) phases all exhibit a second order Jahn-Teller distortion (SOJT) [32] (Table S2). The SOJT results in a smaller distortion of the M(1) polyhedra for *M'* = W [21] at 25 °C so that the reduced SOJT coupled with the smaller percentage of W(1)/Nb(1)O_4 tetrahedra in $Ba_3W_{1.2}Nb_{0.8}O_{8.6}$ results in a bulk ionic conductivity approximately two orders of magnitude lower than $Ba_3MoNbO_{8.5}$ at 400 °C (Figure 2a).

Upon heating the M(1) atoms displace away from the O(2)/O(3) sites as shown in Supplementary Figure S6. The magnitude of this displacement, *D*, was calculated as previously described [22] and its thermal variation is shown in Figure S7. The displacement of the M(1) site away from the mobile oxygen ion reduces the motional enthalpy required for the mobility of the oxide ions, further enhancing the ionic conductivity. This would suggest that the combination of an enhanced structural rearrangement and relaxation coupled with the change in charge carriers in the $BaO_{2.6}$ layers (as a result of the increased oxygen content) results in a bulk ionic conductivity comparable to $Ba_3MoNbO_{8.5}$ at 600 °C.

CONCLUSIONS

In summary the oxide ion conductor $Ba_3W_{1.2}Nb_{0.8}O_{8.6}$ has been synthesised. Significant oxide ion conductivity is observed at 600 °C and there is no evidence of an electronic component in 5% H_2/N_2. Increasing the oxygen concentration in $Ba_3W_{1+x}Nb_{1-x}O_{8.5+x/2}$ enhances the low temperature (400 °C) conductivity. The results reported here demonstrate that $Ba_3M'M''O_{8.5}$

hexagonal perovskite derivatives that crystallise in the 9R/palmierite hybrid structure have the propensity to rearrange so that the ratio of (M'/M'')O_4 tetrahedra to (M'/M'')O_6 octahedra increases upon heating to 600 °C. Further investigation of $Ba_3M'M''O_{8.5}$ hexagonal perovskite derivatives is warranted to find the optimum combination of charge carriers and (M'/M'')O_4:(M'/M'')O_6 ratio.

ASSOCIATED CONTENT

Supporting Information. The supporting information includes tables of crystallographic data, figures showing electrical data, the variation of the angle variance of the M(1)O_4 tetrahedra and M(1)O_6 octahedra, selected bond lengths and the displacement upon heating.

AUTHOR INFORMATION

Corresponding Author

*a.c.mclaughlin@abdn.ac.uk

Tel: 0044 1224272924; Fax: 0044 1224272921

Author Contributions

The manuscript was written through contributions of all authors. All authors have given approval to the final version of the manuscript.

ACKNOWLEDGMENT

This research was supported by the University of Aberdeen and EPSRC (research grant EP/L002493/1). We also acknowledge the UK Science and Technology Facilities Council (STFC) for provision of beamtime at ISIS and the ILL.

References

1. Steele, B. C. H. Oxygen ion conductors and their technological applications. *Mater. Sci. Eng. B,* **1992**, *13*, 79-87.

2. Goodenough, J. B. Oxide-Ion Electrolytes. *Annu. Rev. Mater. Res.*, **2003**, *33*, 91-128.

3. Malavasi, L.; Fisher, C. A. J.; Islam, M. S. Oxide-ion and proton conducting electrolyte materials for clean energy applications: structural and mechanistic features. *Chem. Soc. Rev.,* **2010**, *39*, 4370-4387.

4. Skinner, S. J.; Kilner, J. A. Oxygen ion conductors. *Materials Today,* **2003**, *6*, 30-37.

5. Yamamoto, O. Solid oxide fuel cells: fundamental aspects and prospects. *Electrochim. Acta,* **2000**, *45*, 2423-2435.

6. Wachsman, E. D.; Lee, K. T. Lowering the temperature of solid oxide fuel cells. *Science,* **2011**, *334*, 935-939.

7. Singhal, S. C. Advances in solid oxide fuel cell technology. *Solid State Ionics,* **2000**, *135*, 305-313.

8. Fergus, J. W. Electrolytes for solid oxide fuel cells. *J. Power Sources,* **2006**, *162*, 30-40.

9. Navrotsky, A. Thermodynamics of solid electrolytes and related oxide ceramics based on the fluorite structure. *J. Mater. Chem.,* **2010**, *20*, 10577-10587.

10. Lacorre, P.; Goutenoire, F.; Bohnke, O.; Retoux, R.; Laligant, Y. Designing fast oxide-ion conductors based on $La_2Mo_2O_9$. *Nature*, **2000**, *404*, 856-858.

11. Sammes, N. M.; Tompsett, G. A.; Näfe, H.; Aldinger, F. Bismuth based oxide electrolytes—structure and ionic conductivity. *J. Eur. Ceram. Soc.,* **1999**, *19*, 1801-1826.

12. Kendrick, E.; Islam, M. S.; Slater, P. R. Developing apatites for solid oxide fuel cells: insight into structural, transport and doping properties. *J. Mater. Chem.*, **2007**, *17*, 3104-3111.

13. Ishihara, T.; Matsuda, H.; Takita, Y. Doped $LaGaO_3$ perovskite type oxide as a new oxide ionic conductor. *J. Am. Chem. Soc.*, **1994**, *116*, 3801-3803.

14. Li, M.; Pietrowski, M. J.; De Souza, R. A.; Zhang, H.; Reaney, I. M.; Cook, S. N.; Kilner, J. A.; Sinclair, D. C. A family of oxide ion conductors based on the ferroelectric perovskite $Na_{0.5}Bi_{0.5}TiO_3$. *Nature Mater*., **2014**, *13*, 31-35.

15. Fujii, K.; Esaki, Y.; Omoto, K.; Yashima, M.; Hoshikawa, A.; Ishigaki, T.; Hester, J. R. New perovskite related structure family of oxide ion conducting materials $NdBaInO_4$. *Chem. Mater*., **2014**, *26*, 2488–2491.

16. Kuang, X.; Allix, M.; Ibberson, R. M.; Claridge, J. B.; Niu, H.; Rosseinsky M. J. Oxygen Vacancy Ordering Phenomena in the Mixed-Conducting Hexagonal Perovskite $Ba_7Y_2Mn_3Ti_2O_{20}$ *Chem. Mater.,* **2007**, *19*, 2884-2893.

17. Ling, C. D.; Avdeev, M.; Kharton, V. V.; Yaremchenko, A. A.; Macquart, R. B.; Hoelzel, M. Structures, Phase Transitions, Hydration, and Ionic Conductivity of $Ba_4Ta_2O_9$. *Chem. Mater.,* **2010**, *22*, 532-540.

18. Ling, C. D.; Avdeev, M.; Kutteh, R.; Kharton, V. V.; Yaremchenko, A. A.; Fialkova, S.; Sharma, N.; Macquart, R. B.; Hoelzel, M.; Gutmann, M. Structures, Phase Transitions, Hydration, and Ionic Conductivity of $Ba_4Nb_2O_9$. *Chem. Mater.,* **2009**, *21*, 3853-3864.

19. Dunstan, M. T.; Pavan, A. F.; Kharton, V. V.; Avdeev, M. ; Kimpton, J. A.; Kolotygin, V. A.; Tsipis. E. V.; Ling, C. D. Phase behavior and mixed ionic–electronic conductivity of $Ba_4Sb_2O_9$. *Solid State Ionics,* **2013**, *235*, 1-7.

20. Fop, S.; Skakle, J. M.; McLaughlin, A. C.; Connor, P. A.; Irvine, J. T. S.; Smith, R. I.; Wildman, E. J. . Oxide ion conductivity in the hexagonal perovskite derivative $Ba_3MoNbO_{8.5}$. *J. Am. Chem. Soc.*, **2016**, *138*, 16764-16769.

21. McCombie, K. S.; Wildman, E. J.; Fop, S.; Smith, R. I.; Skakle, J. M. S.; Mclaughlin, A. C. The crystal structure and electrical properties of the oxide ion conductor $Ba_3WNbO_{8.5}$ *J. Mater. Chem. A*, **2018**, *6,* 5290-5295.

22. Fop, S.; Wildman, E. J.; Irvine, J. T. S.; Connor, P. A.; Skakle, J. M.; Ritter, C.; McLaughlin, A. C. Investigation of the Relationship between the Structure and Conductivity of the Novel Oxide Ionic Conductor $Ba_3MoNbO_{8.5}$. *Chem. Mater.*, **2017**, *29*, 4146-4152.

23. Fop, S.; Wildman, E. J.; Skakle, J. M. S.; Ritter, C.; McLaughlin, A. C. Electrical and Structural Characterization of $Ba_3Mo_{1-x}Nb_{1+x}O_{8.5-x/2}$: The Relationship between Mixed Coordination, Polyhedral Distortion and the Ionic Conductivity of $Ba_3MoNbO_{8.5}$ *Inorg. Chem.*, **2017**, *56*, 10505-10512.

24. Larson, A. C.; Von Dreele, R. B. General structure analysis system (GSAS). Los Alamos National Laboratory Report LAUR 86-748 (1994).

25. Toby, B. H. EXPGUI, a graphical user interface for GSAS. *J. Appl. Cryst.*, **2001**, *34*, 210-213.

26. Kemmler-Sack, S.; Treiber U. Über hexagonale Perowskite mit Kationenfehlstellen. XXVIII. Die Struktur der rhomboedrischen 9 L-Stapelvarianten $Ba_3W^{VI}_{2-x}Nb^{V}_{x}\square O_{9-x/2}\square_{x/2}$. *Z. Anorg. Allg. Chem.*, **1981**, *478*, 198-204.

27. Bylichkina, T.I.; Soleva, L.I.; Pobedimskaya, E.A.; Porai Koshits, M.A.; Belov, N.V. Crystal structures of Ba-molybdate and Ba-tungstate. *Kristallografiya*, **1970**, *15*, 165-167.

28. Kemmler-Sack, S.; Treiber, U. Strukturbestimmung an $Ba_9Nb_6WO_{27}$ - der ersten Stapelvariante eines rhomboedrischen 27 L-Typs. *Zeitschrift fuer Anorganische und Allgemeine Chemie*, **1980,** *462*, 166-172.

29. Irvine, J. T. S.; Sinclair, D. C.; West, A. R. Electroceramics: Characterization by Impedance Spectroscopy. *Adv. Mater.*, **1990**, *2*, 132-138.

30. Wang, S.; Zhao, F.; Zhang, L.; Chen, F. Synthesis of $BaCe_{0.7}Zr_{0.1}Y_{0.1}Yb_{0.1}O_{3-\delta}$ proton conducting ceramic by a modified Pechini method. *Solid State Ionics*, **2012**, *213*, 29-35.

31. Bernasconi, A.; Tealdi, C.; Malavasi, L. High-Temperature Structural Evolution in the $Ba_3Mo_{(1-x)}W_xNbO_{8.5}$ System and Correlation with Ionic Transport Properties *Inorg. Chem.,* **2018**, *57*, 6746-6752.

32. Kunz, M.; Brown, D. I. Out-of-center distortions around octahedrally coordinated d^0 transition metals *J. Solid State Chem.*, **1995**, *115*, 395-406.

For Table of Contents Only

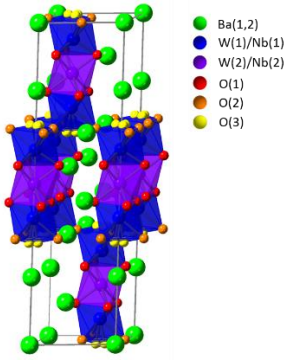

TOC synopsis: Upon heating a structural rearrangement of $Ba_3W_{1.2}Nb_{0.8}O_{8.6}$ occurs resulting in a crystal structure containing 45.5% tetrahedra at 600 °C. The increase in the proportion of $(W/Nb)O_4$ tetrahedra creates a lower energy transition pathway for the transport of O^{2-} ions and enhances the conductivity.